International Journal of Heat and Mass Transfer 52 (2009) 3634–3644

Contents lists available at ScienceDirect

International Journal of Heat and Mass Transfer

journal homepage: www.elsevier.com/locate/ijhmt

Flow boiling in horizontal flattened tubes: Part I – Two-phase frictional pressure drop results and model

Jesús Moreno Quibén [a,b], Lixin Cheng [a,c], Ricardo J. da Silva Lima [a], John R. Thome [a,*]

[a] Laboratory of Heat and Mass Transfer (LTCM), Faculty of Engineering (STI), École Polytechnique Fédérale de Lausanne (EPFL), Station 9, CH-1015 Lausanne, Switzerland
[b] Wolverine LDA, Apartado 21-4740 Esposende, Portugal
[c] School of Engineering, University of Aberdeen, King's College, Aberdeen, AB24 3UE Scotland, UK

ARTICLE INFO

Article history:
Received 26 November 2008
Accepted by 17 December 2008

Keywords:
Flow boiling
Two-phase flow
Diabatic
Frictional pressure drop
Flattened tube
Flow patterns
Phenomenological
Experiment
Model
R22
R410A

ABSTRACT

Experiments of diabatic two-phase pressure drops in flow boiling were conducted in four horizontal flattened smooth copper tubes with two different heights of 2 and 3 mm. The equivalent diameters of the flat tubes are 8.6, 7.17, 6.25, and 5.3 mm. The working fluids are R22 and R410A, respectively. The test conditions are: mass velocities from 150 to 500 kg/m^2 s, heat fluxes from 6 to 40 kW/m^2 and saturation temperature of 5 °C (reduced pressures p_r are 0.12 for R22 and 0.19 for R410A). The experimental results of two-phase pressure drops are presented and analyzed. Furthermore, the predicted two-phase frictional pressure drops by the flow pattern based two-phase pressure drop model of Moreno Quibén and Thome [J. Moreno Quibén, J.R. Thome, Flow pattern based two-phase frictional pressure drop model for horizontal tubes, Part I: Diabatic and adiabatic experimental study, Int. J. Heat Fluid Flow 28 (2007) 1049–1059; J. Moreno Quibén, J.R. Thome, Flow pattern based two-phase frictional pressure drop model for horizontal tubes, Part II: New phenomenological model, Int. J. Heat Fluid Flow 28 (2007) 1060–1072] using the equivalent diameters were compared to the experimental data. The model, however, underpredicts the flattened tube two-phase frictional pressure drop data. Therefore, correction to the annular flow friction factor was proposed for the flattened tubes and now the method predicts 83.7% of the flattened tube pressure drop data within ±30%. The model is applicable to the flattened tubes in the test condition range in the present study. Extension of the model to other conditions should be verified with experimental data.

1. Introduction

Flattened tube heat exchangers have a potential use in a wide range of industrial applications: air-conditioning, heat pump and refrigeration systems, automotive radiators, and fuel cell engines, etc. Compared to a circular tube, a flattened tube has a higher surface-to-cross-sectional flow area ratio, which may be used to enhance the heat transfer rate and increase the compactness of heat exchangers. For example, flattened heat transfer tubes can greatly reduce the refrigerant charge in direct-expansion evaporators and condensers and thus provide more compact heat exchanger design. Furthermore, potential advantages of flattened tube profiles are reduced air-side pressure drop and increased air-side heat transfer. Flattened heat transfer tubes in the present study refer to plain round tubes that have been extruded flat on top and bottom and remain round at the two ends as shown by the photo in Fig. 1.

So far, there are very limited studies on two-phase flow and heat transfer in flattened tubes in the literature. Wilson et al. [1] investigated refrigerant charge, two-phase pressure drop and heat transfer during condensation of refrigerants R134a and R410A in several flattened tubes. Their results show significant reduction in refrigerant charge as a tube is flattened. They also indicate enhancement of condensation heat transfer and an increase of pressure drop in the flattened tubes. Krishnaswamy et al. [2] investigated condensation heat transfer of steam-air mixtures in a horizontal flattened tube. They also proposed a simple heat transfer model. Their model predicts their data satisfactorily. Koyama et al. [3] conducted experiments on two-phase pressure drop and heat transfer of condensation of refrigerant R134a in multi-port extruded flattened tubes with hydraulic diameters of 1.114 and 0.807 mm. They concluded that to establish a prediction method of the pressure drop and heat transfer characteristics of pure refrigerant condensing in a small diameter tube, more experimental data for small diameter tubes should be investigated by considering the following terms: (1) flow patterns, (2) the effect of tube diameter, and (3) the interaction effect among the vapor shear stress and the gravitational acceleration and the surface tension. As for flow boiling in flattened tubes, however, there is no study available in the

* Corresponding author. Tel.: +41 21 693 5981; fax: +41 21 693 5960.
E-mail addresses: jmoreno@wolverine.com.pt (J.M. Quibén), lixincheng@hotmail.com (L. Cheng), ricardo.lima@epfl.ch (R.J. da Silva Lima), john.thome@epfl.ch (J.R. Thome).

0017-9310/$ - see front matter © 2009 Elsevier Ltd. All rights reserved.
doi:10.1016/j.ijheatmasstransfer.2008.12.032

Nomenclature

A	cross-sectional area of flow channel (m^2)
C	correction factor
c_p	specific heat at constant pressure (J/kg K)
D	internal tube diameter (m)
$\frac{di_{wat}}{dz}$	water enthalpy change over distance, dz (J/kg)/m
f	friction factor
G	total vapor and liquid two-phase mass flux (kg/m^2 s)
g	gravitational acceleration (=9.81 m/s^2)
H	height of flattened tube (m)
i	enthalpy (J/kg)
i_{LV}	latent heat of vaporization (J/kg)
L	tube length (m)
m	mass flow rate (kg/s)
N	number of data points
P	perimeter of test tube (m)
p	pressure (bar)
p_r	reduced pressure ($=p/p_{crit}$)
Q	transferred heat (W)
q	heat flux (W/m^2)
Re_V	vapor phase Reynolds number ($=GxD_e/\mu_V\varepsilon$)
T	temperature (K)
t	tube wall thickness (m)
u	mean velocity (m/s)
W	width of flattened tube (m)
We_L	liquid Weber number ($=\rho_L u_L^2 D_e/\sigma$)
x	vapor quality
z	distance from the tube inlet (m)

Greeks

Δp	pressure drop (Pa)
δ	liquid film thickness (m)
ε	cross-sectional vapor void fraction
μ	dynamic viscosity (N s/m^2)
ρ	density (kg/m^3)
σ	surface tension (N/m); standard deviation (%)
ξ_i	relative error (%)
$\bar{\xi}$	average error (%)
$\lvert\bar{\xi}\rvert$	mean error (%)

Subscripts

A	annular flow
crit	critical
e	equivalent
exp	experimental
ext	external
f	frictional
h	hydraulic
i	data point
in	inlet
L	liquid
LV	liquid–vapor
m	momentum
out	outlet
pred	predicted
preheater	preheater
ref	refrigerant
s	static
sat	saturation
t	total
V	vapor
wat	water
wet	wetted

literature. In order to design a flattened tube evaporator, it is important to understand and predict the two-phase flow and flow boiling heat transfer characteristics inside horizontal flattened tubes. In particular, in the case of a flattened tube having a very small height between the top and bottom, the confinement of such a tube will greatly affect two-phase pressure drop and heat transfer characteristics [4–7]. In the present study, experimental investigation of two-phase pressure drops and flow boiling heat transfer with refrigerants R22 and R410A in four flattened smooth copper tubes with 2 and 3 mm heights is performed. In Part I, experimental results of two-phase frictional pressure drops are presented and analyzed. Furthermore, a modified flow pattern based phenomenological two-phase flow frictional pressure drop model for these flattened tubes is presented. Experimental investigation of flow boiling heat transfer characteristics of these fluids and an updated flow pattern based flow boiling heat transfer model are presented in Part II.

Flow patterns are very important in understanding the very complex two-phase flow phenomena and heat transfer trends in flow boiling [8]. As the predictions of two-phase flow frictional pressure drops with the leading methods often cause errors of more than 50% [9], efforts are increasingly being made to improve the accuracy of two-phase flow pressure drop predictions. In addition, the empirical two-phase pressure drop prediction methods do not contain any flow pattern information, which is intrinsically related to the two-phase frictional pressure drop. As opposed to such completely empirical two-phase pressure drop methods, a flow pattern based phenomenological model relating the flow patterns to the corresponding two-phase flow pressure drops is a more promising approach [8,9]. A new flow pattern based phenomenological model of two-phase frictional pressure drops was recently developed by Moreno Quibén and Thome [10–12]. The model physically respects the two-phase flow structure of the various flow patterns while maintaining a degree of simplicity as well.

Fig. 1. Photograph of round and flattened tubes.

The model predicts their experimental data well. Cheng et al. [13,14] modified the model to improve its accuracy for CO_2. Recently, da Silva Lima et al. [15] compared the model of Moreno Quibén and Thome to their ammonia two-phase pressure drop data and found the model predicted their ammonia data well.

In Part I of the present study, first, experiments of diabatic two-phase pressure drops and flow boiling heat transfer were conducted in four horizontal flattened copper tubes with two different heights of 2 and 3 mm. The experimental two-phase frictional pressure drop results are presented and analyzed. Furthermore, the flow pattern based two-phase frictional pressure drop model of Moreno Quibén and Thome [10–12] was modified to predict the two-phase pressure drops in the flattened tubes.

2. Test facility, test sections and measurement system

The test facility is schematically shown in Fig. 2. It consists of a refrigerant circulating circuit, a heating water circuit for the test section and a cooling water-glycol mixture circuit for the condenser. The test fluids are R22 and R410A. The test refrigerant is circulated from the condenser to the system by an oil-free magnetically driven gear type pump. First, the refrigerant flows through a Coriolis mass flow meter. Then, it goes into a series of horizontal electrical preheaters. Next, the refrigerant enters the test section where it is heated by the counter-current flow of hot water in the annulus of a double pipe system and is thus evaporated. Finally, it flows back to the condenser. The liquid–vapor reservoir in the test loop is used to stabilize the system and to obtain a desired operation pressure. All the fluid pipes in the system are well insulated. All the tube connections have a smooth interface to avoid disturbing the flow.

The test tubes include four flattened copper tubes and two round tubes (for the validation of the test facility) which are shown in Figs. 1 and 3. The test flattened tube number and the dimensions indicated in Fig. 3 are given in Table 1, where the hydraulic and equivalent diameters are defined by Eqs. (1) and (4), respectively. For the flattened tube, refer to Fig. 3, the hydraulic diameter is defined as

$$D_h = \frac{4A}{P_{wet}}, \tag{1}$$

where the cross-sectional area A and wetted perimeter are calculated, respectively, by

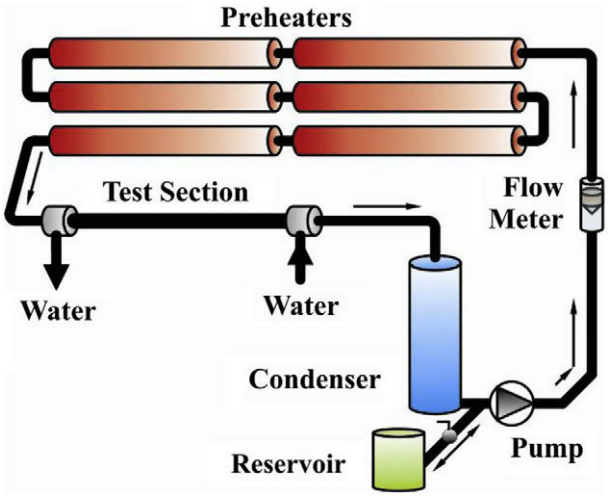

Fig. 2. Schematic of the test facility.

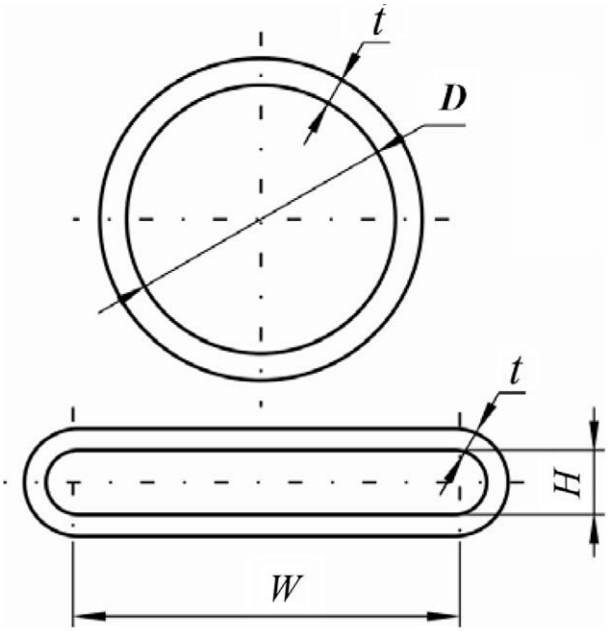

Fig. 3. Cross-section of round and flattened tubes.

Table 1
Round and flattened tube dimensions (mm).

Tube	H	W	t	D	D_e	D_h
Flattened tube No. 1	2	18.6	1.02		7.17	3.71
Flattened tube No. 2	3	17	0.76		8.6	5.35
Flattened tube No. 3	2	9.44	1.02		5.3	3.5
Flattened tube No. 4	3	7.87	0.86		6.25	4.88
Round tube			1.015	13.84		
Round tube			0.765	8		

$$A = \frac{\pi H^2}{4} + HW, \tag{2}$$

$$P_{wet} = \pi H + 2W. \tag{3}$$

The equivalent diameter is defined as

$$D_e = \sqrt{\frac{4A}{\pi}}. \tag{4}$$

The test section is schematically shown in Fig. 4. It is a double pipe counterflow heat exchanger, where the test flattened tube is placed as the internal pipe. The refrigerant flows inside the internal flattened tube and the hot-water mixture flows in a counterflow direction in the annulus of the double pipe heat exchanger. As indicated in Fig. 4, T refers to temperature, P to absolute pressure, DP to differential pressure, W to water, R to refrigerant and the numbers refer to the different sensors. The cross-sectional distribution of the thermocouples for both hot water and wall temperature measurements and their axial position and number at each measurement section are shown in Fig. 4.

The measured parameters include mass flow rate, wall temperatures, fluid temperatures, inlet and outlet absolute pressures, and differential pressure across the test section. Mass flow rate in the test tube was measured by the Coriolis mass flow meter. The measurement uncertainty is ±0.15%.

Temperatures were measured by thermocouples. For hot-water temperature, the thermocouples have a diameter of 0.5 mm and the thermocouple tips are fixed at 0.3 mm from the outside wall of the flattened tube. For wall temperature measurement, the

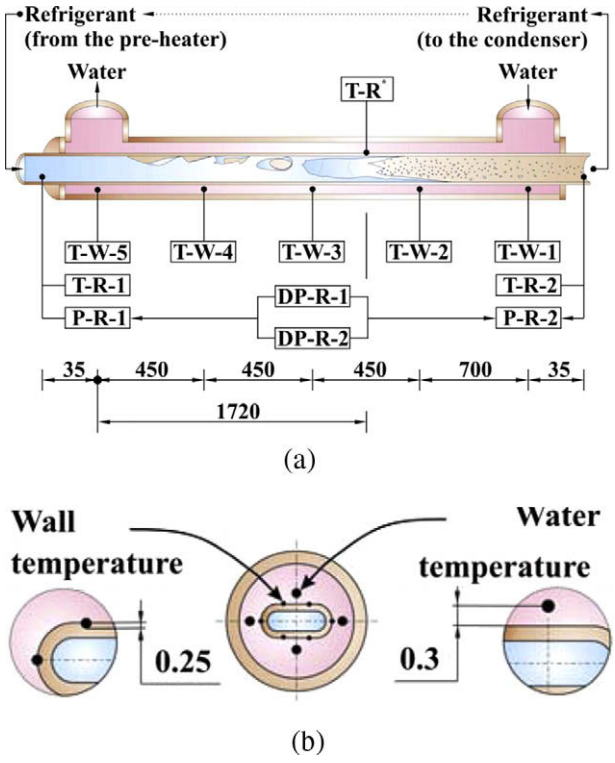

Fig. 4. (a) Schematic of the horizontal test section. (b) Schematic of the measurement points in the cross-sectional sections with the indication of the position of the thermocouple and its respective identification.

thermocouples were 0.25 mm in diameter and brazed into grooves of 15 mm long and 0.25 mm deep on the outside surface of the tested tube. All thermocouples were carefully and accurately calibrated in situ to an accuracy of ±0.03 °C compared to two precision thermometers of Omega Engineering, model DP251, placed at the entrance and exit of the channel in the hot-water side of the test section (annulus). The temperature measurements during the calibration were made at steady, adiabatic conditions for a positive and negative step change of temperature of the water over a temperature range larger than the experimental conditions during the experimental campaign.

The inlet and outlet absolute pressures were measured by two pressure transducers P-R-1 and P-R-2. The pressure transducers were calibrated with a very accurate balance over the range from 1 to 25 bars. After calibration, the values of both pressure transducers installed in the test section were compared in a static pressure test. The results showed good agreement. The saturation temperature T_{sat} of the fluid in the test section was obtained from absolute pressure measurements (P-R-1 and P-R-2 in made at the extremities of the test section, thus avoiding disturbing measurements with intrusive thermocouples. The end point measurements were corroborated by the inlet and outlet temperature measurements, T-R-1 and T-R-2, respectively. The local refrigerant saturation temperature T_{sat} at the position of T-R* in Fig. 4 was determined by the local saturation pressure p, which was calculated by linear interpolation between the inlet and outlet pressures. The assumption of a linear pressure distribution over the length of the test section is valid as the vapor quality variation in the test section is small (generally less than 0.01).

The two-phase pressure drops were measured using two differential pressure transducers, DP-R-1 and DP-R-2, each one covering different pressure drop ranges: low (0–40 mbar) and medium (0–500 mbar), which allows maintaining a low level of uncertainty. Both had an accuracy of ±0.05% F.S. When the pressure drop exceeded the range of the differential pressure transducers, the pressure drop was obtained from the difference between the absolute pressure transducers, P-R-1 and P-R-2 in Fig. 4. The total distance between the two pressure (also differential pressure) taps was 2.12 m. The most appropriate sensor was used in each case and a self-check was available at the transition from one to the other. As the smallest and largest two-phase pressure drops measured in this study were 1.63 and 737 mbar, respectively, the corresponding experimental accuracies ranged from ±0.54% to ±1.22%, respectively. The absolute pressure drop uncertainty was ±20 mbar.

The test runs were set in the range of mass velocities from 150 to 500 kg/m^2 s, heat fluxes from 6 to 40 kW/m^2 and saturation temperature of 5 °C. For each test run, these parameters were manually controlled to achieve the desired test conditions. The measurements obtained with a National Instruments data acquisition system were monitored through a Personal Computer. Each experimental point resulted from the average of 10 acquisition cycles. Each acquisition cycle corresponded to an average from 100 acquisitions made in approximately 0.02 s. All measurements were made at steady state conditions.

3. Data reduction and test procedure

In the present study, the physical properties were obtained from REFPROP of NIST Version 6.01 [16].

The heat flux q is controlled by the temperature of the hot water. The temperatures of the hot water were measured at five positions along the test section (T-W-1, T-W-2, T-W-3, T-W-4, T-W-5, see Fig. 4), which is used to determine its enthalpy:

$$i_{wat}(z) = c_{p\text{-}wat} T_{wat}(z). \tag{5}$$

The external heat flux along an elementary length dz is calculated as

$$q_{ext}(z) = \frac{m_{wat}}{P_{ext}} \left(\frac{di_{wat}}{dz} \right) \tag{6}$$

and thereby the local heat flux based on the flatten tube internal heated perimeter is calculated as

$$q(z) = q_{ext}(z) \left(\frac{P_{ext}}{P_{wet}} \right) = \frac{m_{wat}}{P_{wet}} \left(\frac{di_{wat}}{dz} \right). \tag{7}$$

The water local temperature obtained at the measurement sections corresponds to the mean from four or six thermocouples circumferentially disposed in the annulus of the double pipe. The cross-sectional distribution of the thermocouples is shown in Fig. 4(b).

The vapor quality x is calculated by an energy balance over the preheater and the diabatic test section. Hence, the vapor quality at position z along the test section is calculated by

$$x(z) = \frac{Q_{preheater} + m_{wat} c_{p\text{-}wat} (T_{wat\text{-}in} - T_{wat}(z))}{m_{ref} i_{LV}(z)}. \tag{8}$$

The total pressure drop of a fluid corresponds to the sum of three components: momentum, frictional and static head:

$$\Delta p_t = \Delta p_s + \Delta p_m + \Delta p_f. \tag{9}$$

The flow is horizontal and thus Δp_s equals 0. Therefore, the frictional pressure drop is obtained by subtracting the momentum pressure drop from the measured pressure drop:

$$\Delta p_f = \Delta p_t - \Delta p_m, \tag{10}$$

where the momentum pressure drop reflects the increase in the kinetic energy of the flow during the evaporation process. The momentum pressure drop is given by the following expression:

$$\Delta p_m = G^2\left\{\left[\frac{(1-x)^2}{\rho_L(1-\varepsilon)}+\frac{x^2}{\rho_V\varepsilon}\right]_{out}-\left[\frac{(1-x)^2}{\rho_L(1-\varepsilon)}+\frac{x^2}{\rho_V\varepsilon}\right]_{in}\right\}, \quad (11)$$

where the void fraction ε was calculated with the drift flux model of Rouhani and Axelsson [17]:

$$\varepsilon = \frac{x}{\rho_V}\left\{[1+0.12(1-x)]\left(\frac{x}{\rho_V}+\frac{1-x}{\rho_L}\right)+\frac{1.18(1-x)[g\sigma(\rho_L-\rho_V)]^{0.25}}{G\rho_L^{0.5}}\right\}. \quad (12)$$

Thus, diabatic experimental frictional pressure drop can be obtained from Eq. (10). Although the variations of the vapor quality x in the diabatic test section are small, the evaluation of the momentum pressure drop is made by piecewise decomposition, between each water temperature measurement section. The diabatic pressure drops are then reported with respect to the mean value in the test section.

The measurement uncertainties were calculated taking into consideration the uncertainty of each element (described in Section 2) accordingly to a propagation of error analysis following the square root of the sum of the difference or RSS method [18]. The resulting maximum uncertainties do not exceed: 2.5% for the heat flux and 0.01 for the vapor quality. The mean experimental error for the heat transfer coefficients is ±6%. The pressure drop uncertainty is always less than ±1.22%.

4. Experimental results and analysis

4.1. Single-phase turbulent flow and heat transfer validation test results

Before the two-phase tests for the flattened tubes, single liquid phase energy balance and turbulent heat transfer in two circular tubes with internal diameters of 8 and 13.84 mm were performed to validate the measurement system in the present study. As shown in Fig. 5, the energy balance error was systematically lower than 2.5%, which confirms that the insulation and measurement are reliable. This assures that the energy balance in flow boiling is reliable. The single-phase experimental heat transfer results were in good agreement with the calculated values by the Dittus–Boelter [19] and Gnielinski [20] correlations as shown in Fig. 6. This confirms that the experimental results on two-phase flow and flow boiling using the test facility and measurement system are accurate and reliable. On the other hand, the single-phase pressure drops measured during these same tests were too small for the differential pressure transducers, which were sized for the larger two-phase pressure drops expected.

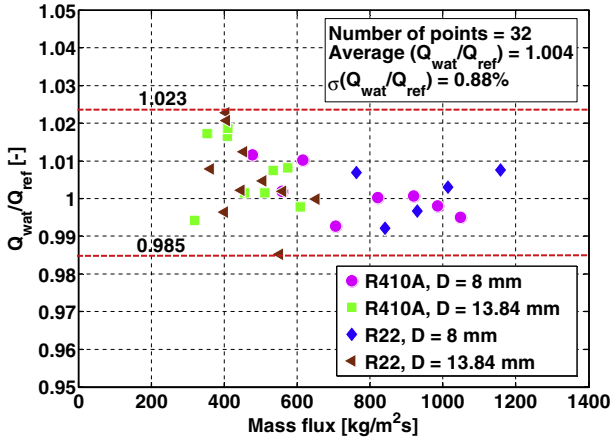

Fig. 5. Energy balance for single-phase heat transfer of R22 and R410A for both 13.84 and 8 mm I.D. round tubes.

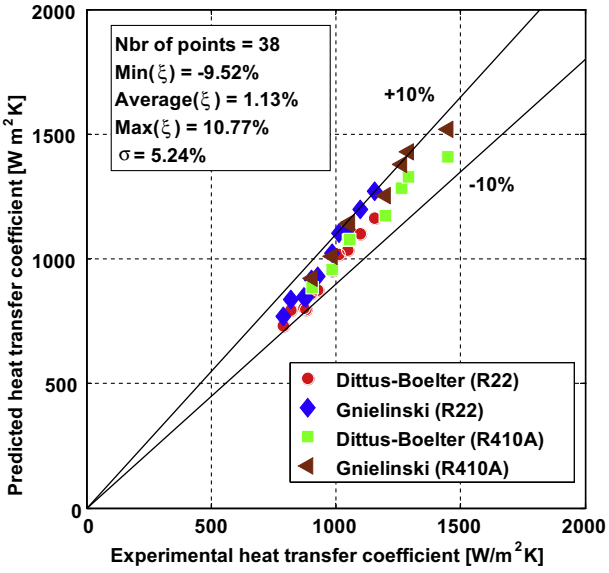

Fig. 6. Predicted versus experimental single-phase heat transfer coefficient for R22 and R410A for the 13.84 mm I.D. round tubes.

4.2. Two-phase frictional pressure drop experimental results

Experiments of diabatic two-phase pressure drops in flow boiling of the test refrigerants were conducted in the four horizontal flattened copper tubes for a wide range of test conditions: mass velocities from 150 to 500 kg/m^2 s, heat fluxes from 6 to 40 kW/m^2 and saturation temperature of 5 °C. Fig. 7 shows the effect of mass flux on the two-phase frictional pressure gradient in the four flattened tubes for R22 and Fig. 8 shows the data for R410A. It can be seen that the frictional pressure gradient increases with increasing mass flux for both refrigerants. Furthermore, it can be seen that R410A has lower frictional pressure gradients than R22 as expected because R410A has a lower liquid–vapor density ratio (lower vapor–liquid specific volume ratio), a lower liquid-vapor viscosity ratio and a lower surface tension than R22.

Fig. 9 shows the effect of heat flux on two-phase frictional pressure gradient for R22 in No. 1 and No. 2 test tubes and for R410A in No. 3 and No. 4 test tubes. It can be seen that heat flux has no effect on the frictional pressure gradient for the same test tube at the same test conditions for both refrigerants. This is consistent with the experimental pressure drop results for several refrigerants in the circular tubes in Moreno Quibén and Thome [10–12] and Silva Lima et al. [15].

Fig. 10 shows the effect of equivalent diameter on the frictional pressure gradient for the same test conditions. In general, the frictional pressure gradient increases with decreasing tube equivalent diameter, that is with decreasing channel height. It should be noted that the two-phase frictional pressure gradient differences for the similar tube equivalent diameters (e.g. D_e = 7.17 and 8.6 mm or D_e = 5.3 and 6.25 mm) are significant although the diameter difference is relatively small. The smaller channel height may result in larger pressure drops due to a confinement effect. The physical explanation should be investigated through flow visualization in the confined channels in the future while such observations were not performed in the present study.

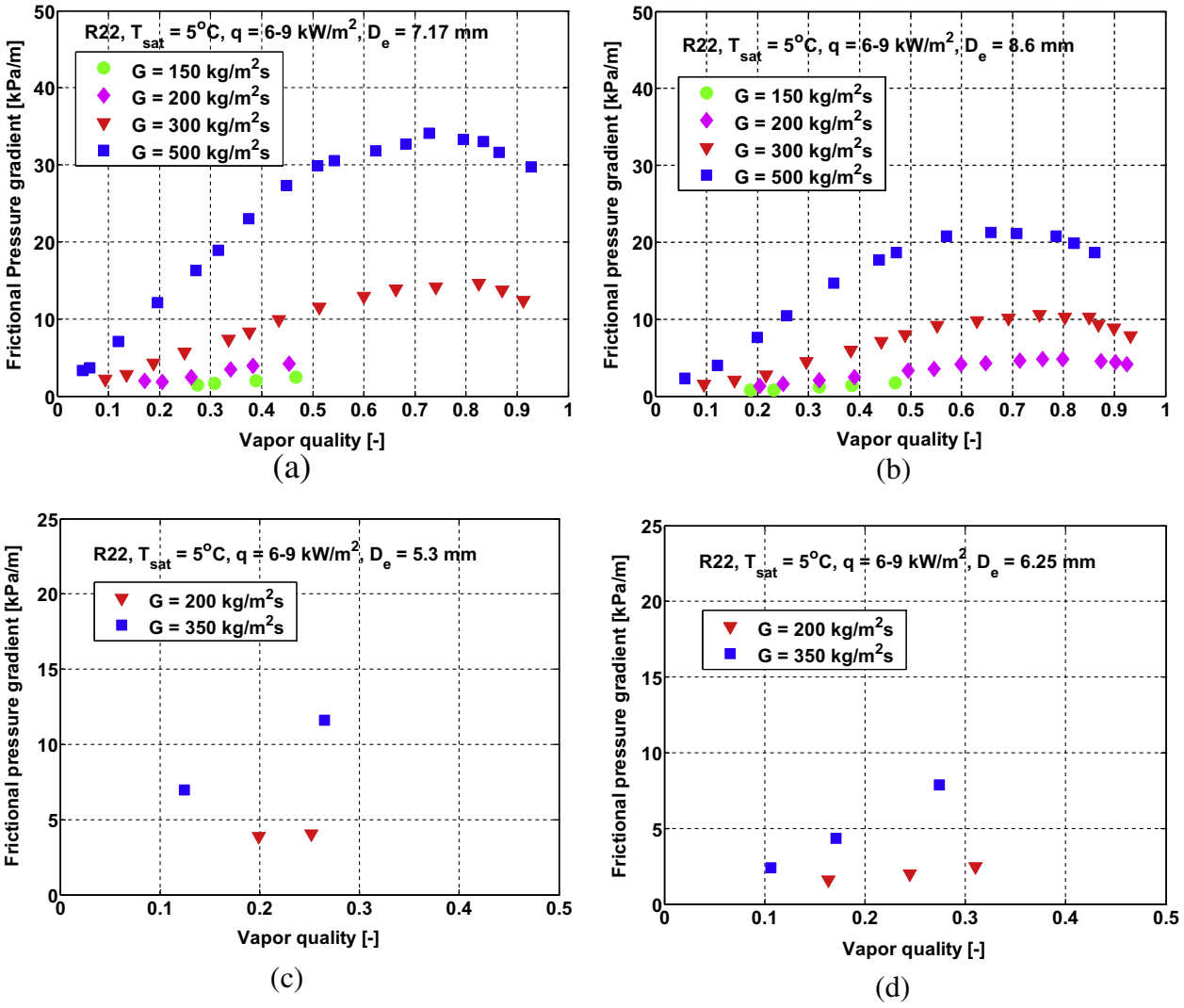

Fig. 7. The effect of mass flux on two-phase frictional pressure gradient for R22: (a) Tube No. 1, (b) Tube No. 2, (c) Tube No. 3, and (d) Tube No. 4.

4.3. Comparison of the experimental data to the flow pattern based two-phase pressure drop model of Moreno Quibén and Thome

Moreno Quibén and Thome [10–12] recently proposed a new flow pattern based phenomenological model of two-phase frictional pressure drops. The model physically respects the two-phase flow structure of the various flow patterns while maintaining a degree of simplicity as well. Their model was developed for R-22, R-410A and R-134a evaporation in horizontal circular tubes and incorporated the flow pattern map of Wojtan et al. [21,22], which is an improved version of the map of Kattan–Thome–Favrat [23]. The model predicted their circular tube experimental data quite well for 8 and 13.84 mm tubes.

Since the same working fluids as those of Moreno Quibén and Thome [10–12] were tested for the flattened tubes in this study, their model is compared to the flattened tube experimental pressure drop data as a first step here, using the round tube map of Wojtan et al. [21,22] to identify the flow regimes in the flattened tubes. As mentioned by Cheng et al. [13,14,24,25] for non-circular channels, equivalent diameters rather than hydraulic diameters should be used in the flow pattern map. Using the equivalent diameter gives the same mass velocity as in the non-circular channel and thus correctly reflects the mean liquid and vapor velocities, something the hydraulic diameter in a two-phase flow does not. Remaining consistent to the flow map, the equivalent diameter is also used in the two-phase pressure drop model. The details of flow map can be found in [21,22]. Fig. 11 shows their map for R22 at the indicated conditions, where different flow regimes are defined.

The details of the circular tube two-phase pressure drop model are given in [10–12]. Comparison of the entire flattened tube two-phase frictional pressure drop data for R22 and R410A to the predicted values by the Moreno Quibén and Thome pressure drop model was made. Fig. 12 shows the variation of the ratio of the experimental to the predicted frictional pressure drops versus vapor quality. The ratios are much higher at lower vapor qualities than those at intermediate vapor qualities and generally larger than for the circular rubes. This effect may be caused by the confined channel height H. In this case, the model does not work for flattened tubes. Therefore, a modification of the model is needed for the flattened tubes.

5. Modified two-phase frictional pressure drop model for flattened tubes and comparisons to experimental data

5.1. Modified frictional pressure drop model for flattened tubes

Since the Moreno Quibén and Thome pressure drop models for other flow regimes except mist flow are all based on the annular

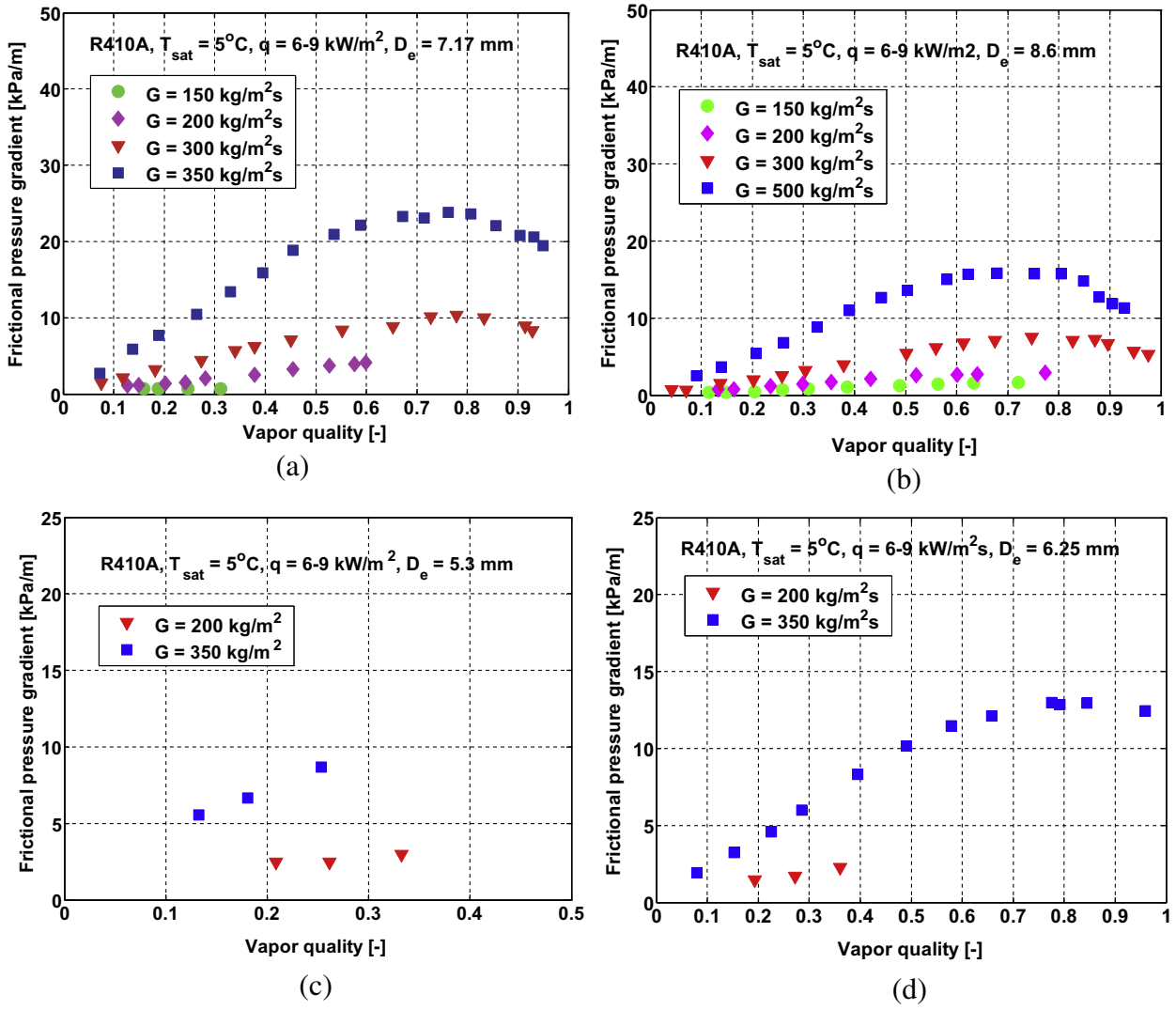

Fig. 8. The effect of mass flux on two-phase frictional pressure gradient for R410A: (a) Tube No. 1, (b) Tube No. 2, (c) Tube No. 3, and (d) Tube No. 4.

flow frictional friction factor, the modification was only made to annular flow frictional factor expression while the others remain unchanged. The modification is as follows. First of all, for non-circular channels, the equivalent diameter D_e is used in the pressure drop model to remain consistent with that in the flow pattern map. Using equivalent diameter gives the same mass velocity as in the actual non-circular channel and thus correctly reflects the mean liquid and vapor velocities, whereas using the hydraulic diameter in a two-phase flow does not. For circular channels, the equivalent diameter D_e equals the actual internal diameter.

The basic equation of the Moreno Quibén and Thome [10–12] pressure drop model for annular flow is as follows:

$$\Delta p_A = 4 f_A \frac{L}{D_e} \frac{\rho_V u_V^2}{2}, \tag{13}$$

where the two-phase flow friction factor of annular flow f_A was modified according the flattened tube experimental data (considering the main parameters which affect the two-phase pressure drops for the flattened tubes) as

$$f_A = C \left[\frac{\delta}{D_e}\right]^{1.2} \left[\frac{(\rho_L - \rho_G) g \delta^2}{\sigma}\right]^{-0.4} \left[\frac{\mu_V}{\mu_L}\right]^{0.08} We_L^{-0.034}, \tag{14}$$

where $C = 0.67$ for circular tubes and $C = 11.5 Re_V^{-0.157}$ for flattened tubes.

The mean velocity of the vapor phase u_V is calculated as

$$u_V = \frac{Gx}{\rho_V \varepsilon}. \tag{15}$$

The void fraction ε is calculated using Eq. (12). The vapor phase Reynolds number Re_V and the liquid phase Weber number We_L based on the mean liquid phase velocity u_L are calculated as

$$Re_V = \frac{GxD_e}{\mu_V \varepsilon}, \tag{16}$$

$$We_L = \frac{\rho_L u_L^2 D_e}{\sigma}, \tag{17}$$

$$u_L = \frac{G(1-x)}{\rho_L (1-\varepsilon)}. \tag{18}$$

5.2. Comparisons of the modified pressure drop model to the experimental data

Fig. 13 shows the comparison of the modified pressure drop model to the experimental data for the flattened tubes at the indicated experimental conditions. The modified model predicts the experimental data quite well. Fig. 14 shows the comparison to

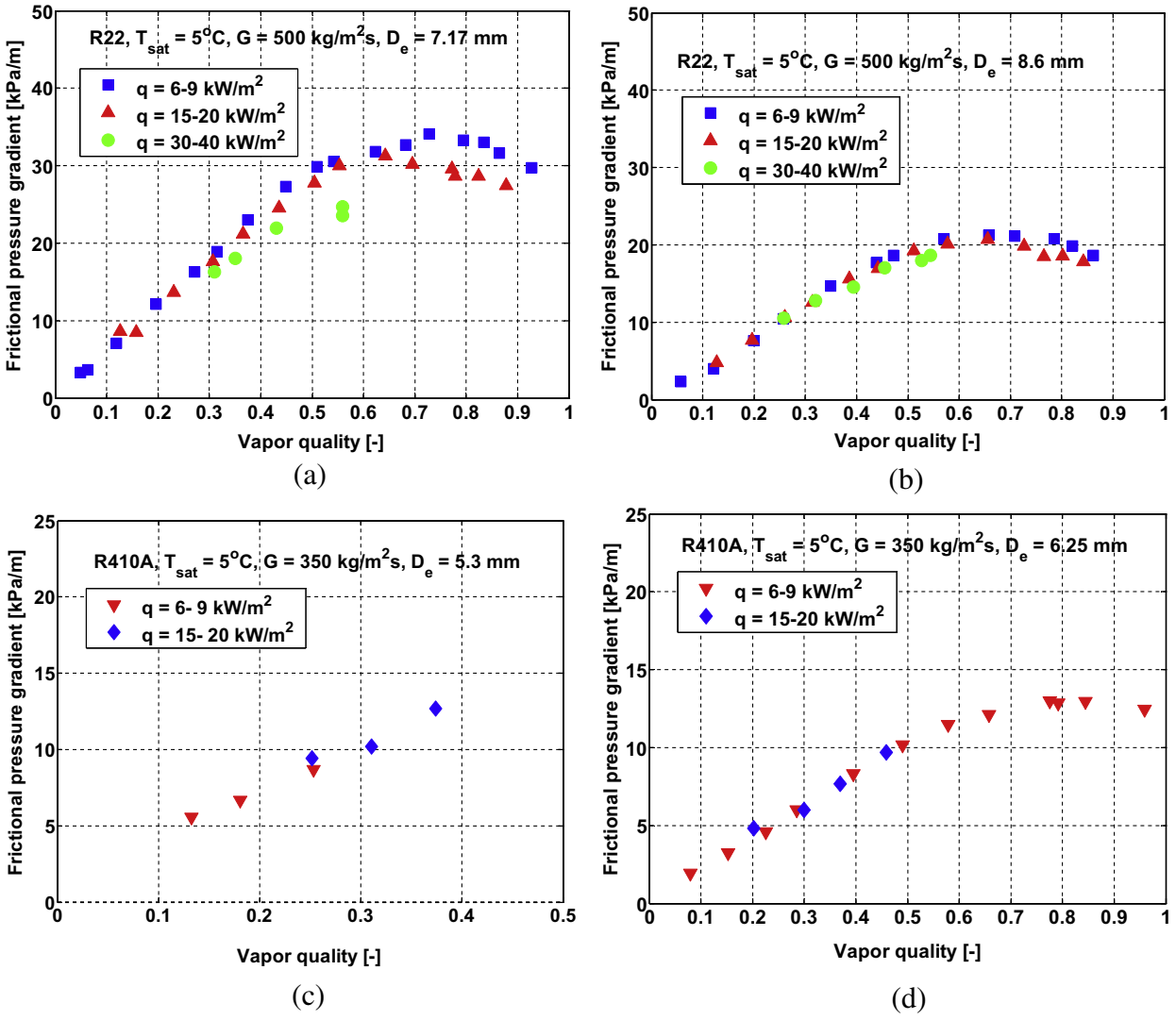

Fig. 9. The effect of heat flux on two-phase frictional pressure gradient: (a) Tube No. 1 for R22, (b) Tube No. 2 for R22, (c) Tube No. 3 for R410A, and (d) Tube No. 4 for R410A.

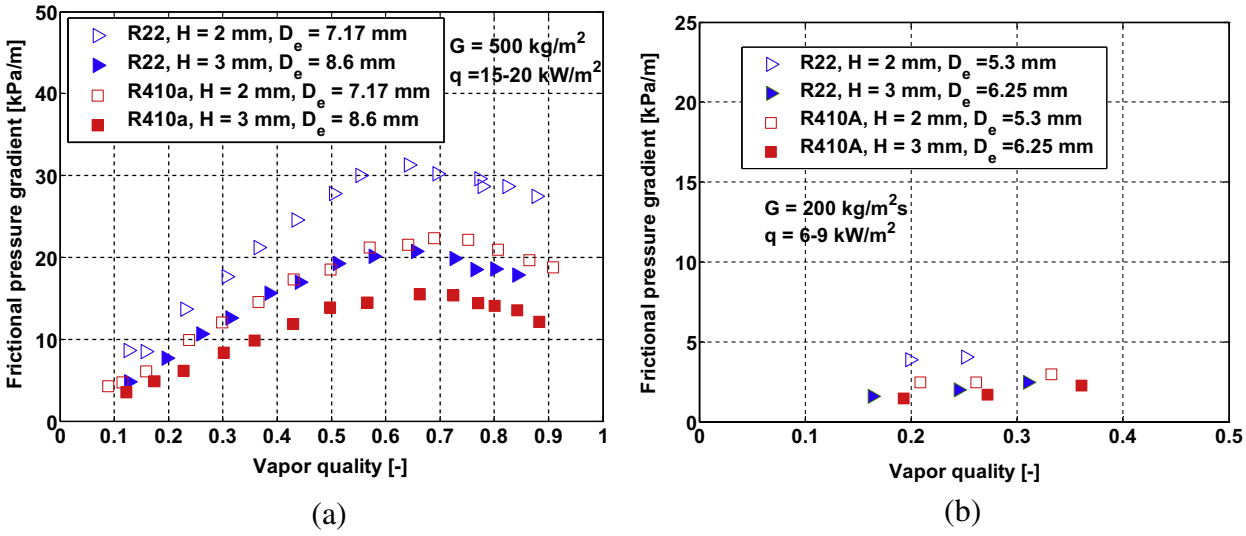

Fig. 10. The effect of channel height on two-phase frictional pressure gradient for R22 and R410A: (a) G = 500 kg/m^2, q = 15–20 kW/m^2 and (b) G = 200 kg/m^2, q = 6–9 kW/m^2.

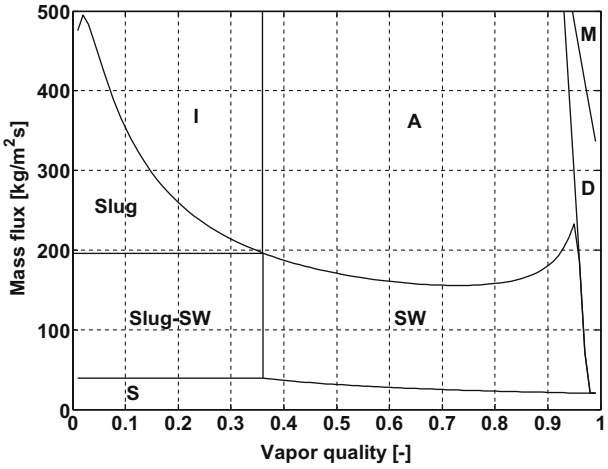

Fig. 11. Flow pattern map for R22 at T_{sat} = 5 °C in a 13.84 mm internal diameter tube at G = 100 kg/m^2 s and q = 2.1 kW/m^2 (S, stratified flow; SW, stratified-wavy flow; I, intermittent flow; A, annular flow; D, dryout region; M, mist flow) [21,22].

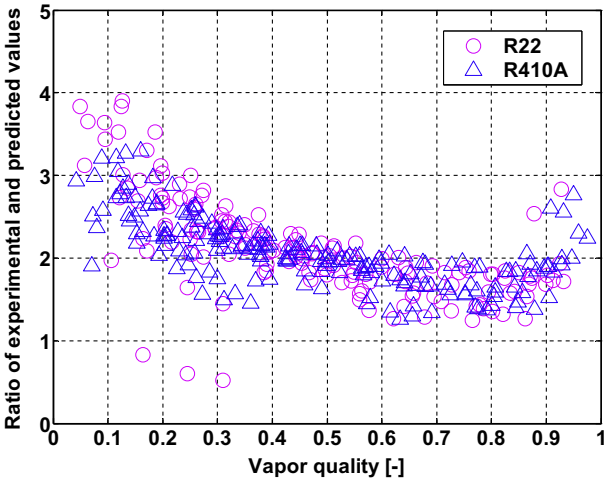

Fig. 12. Experimental and predicted two-phase frictional pressure drop ratios versus vapor qualities for R22 and R410A.

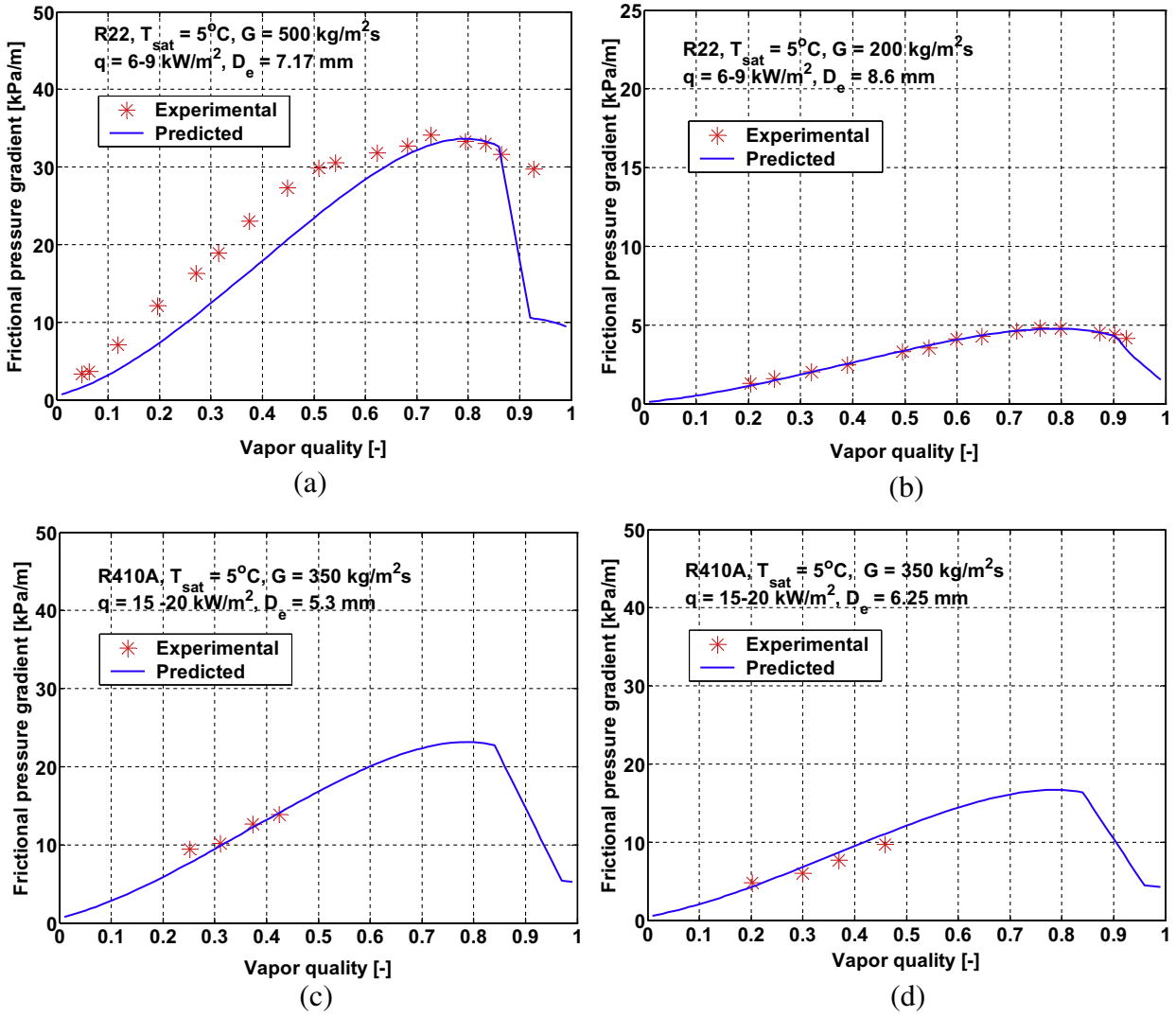

Fig. 13. Comparison of experimental and predicted two-phase frictional pressure gradients: (a) R22 for Tube No. 1, (b) R22 for Tube No. 2, (c) R410A for Tube No. 3, and (d) R410A for Tube No. 4.

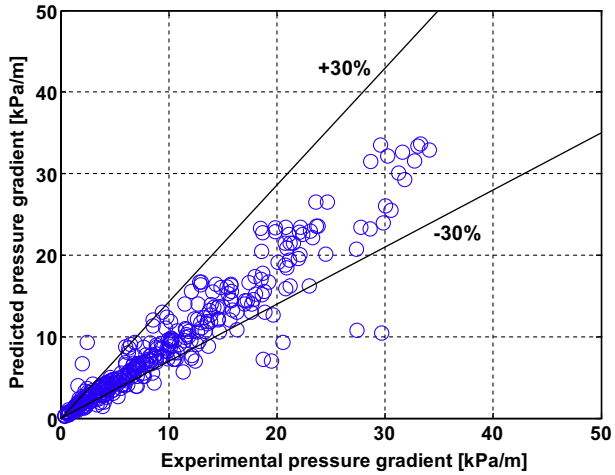

Fig. 14. Comparison of predicted two-phase frictional pressure gradients by the new model to the experimental data for R22 and R410A.

Table 2
Statistical analysis of the two-phase frictional pressure drop predictions for all data points of R22 and R410A according to flow patterns.

Data used for comparison	Experimental data points	Percentage of predicted data points (relative error ξ) within ±30%	Mean error, $\|\overline{\xi}\|$	Standard deviation, σ
Slug-SW	18	66.7%		
SW	10	70%		
I + Slug	139	80.6%		
Annular flow	153	94.8%		
Dryout	30	70%		
Mist flow	5	0		
All data points	355	83.7%	18.2%	38.6%

the entire two-phase pressure drop database for R22 and R410A. The statistical analysis of the comparison of the modified model to the entire database is summarized in Table 2. The analysis is based on relative error ξ_i (the percentage of predicted points within ±30%), mean error $|\overline{\xi}|$ and standard deviation σ, which are respectively calculated as

$$\xi_i = \frac{Predicted - Measured}{Measured}, \tag{19}$$

$$|\overline{\xi}| = \frac{1}{N}\sum_{i=1}^{N}|\xi_i|, \tag{20}$$

$$\sigma = \sqrt{\frac{1}{N}\sum_{i=1}^{N}(\xi_i - \overline{\xi})^2}. \tag{21}$$

As shown in Table 2, the modified two-phase frictional pressure drop model predicts the flattened tube pressure drop data quite well. In addition, a detailed breakdown of the statistical analysis according to flow regimes for the modified pressure drop model is summarized in Table 2. Most of the experimental data points (around 82%) are in annular flow (A), and intermittent and slug (I + Slug) flows. Most of the flow regimes except slug-stratified (Slug-SW) and mist (M) flow regimes are predicted well. Generally, the modified pressure drop model captures the trends in the data as shown in Fig. 13. However, the prediction in the mist flow regime is not satisfactory but this might be caused by the limited data points available. The prediction for slug-stratified-wave (Slug-SW) flow is not satisfactory as well and further experimental data are needed to improve the model in this regime. On the other hand, it is likely that the flow regime transitions in the flattened tubes are somewhat different from those in circular tubes. Therefore, future experimental work is recommended to observe the flow regimes and to better understand the physical mechanisms in the flattened tubes and non-circular channels in general.

6. Conclusions

Experiments of diabatic two-phase pressure drops in flow boiling of R22 and R410A were conducted in four horizontal flattened smooth copper tubes with two different heights of 2 and 3 mm for mass fluxes from 150 to 500 kg/m^2 s, heat fluxes from 6 to 40 kW/m^2 and a saturation temperature of 5 °C. Various parameter effects on the two-phase frictional pressure drops were investigated. From the present study, the following conclusions are obtained:

(1) Heat flux has no significant effect on the two-phase frictional pressure drops.
(2) The circular tube model of Moreno Quibén and Thome [10–12] using the equivalent diameter was compared to the flattened tube experimental data. However, the model significantly underpredicted the flattened tube pressure drop data.
(3) A modified model, correcting the annular flow friction factor of Moreno Moreno Quibén and Thome, was proposed for the flattened tubes and it predicts the flattened tube pressure drop data quite well overall for all flow regimes except for mist flow. The model is applicable to the flattened tubes in the test condition range in the present study. Extension of the model to other conditions should be verified with experimental data.
(4) Future experimental work is recommended to observe the flow regimes to better understand the physical mechanisms of two-phase frictional pressure drops in the flattened tubes and non-circular channels in general.

Acknowledgements

The Laboratory of Heat and Mass Transfer (LTCM) at the École Polytechnique Fédérale de Lausanne (EPFL) wishes to thank ARTI for sponsoring this project with contract ARTI-21CR/605-20040-01. LTCM wishes to also thank Wolverine Tube Inc. for providing the extruded flattened tubes for the tests.

References

[1] M.J. Wilson, T.A. Newell, J.C. Chato, C.A. Infante Ferreira, Refrigerant charge, pressure drop and condensation heat transfer in flattened tubes, Int. J. Refrigeration. 26 (2003) 442–451.
[2] S. Krishnaswamy, H.S. Wang, J.W. Rose, Condensation from gas–vapor mixtures in small non-circular tubes, Int. J. Heat Mass Transfer 49 (2006) 1731–1737.
[3] S. Koyama, K. Kuwahara, K. Nakashita, K. Yamamoto, An experimental study on condensation of refrigerant R134a in a multi-port extruded tube, Int. J. Refrigeration 24 (2003) 425–432.
[4] L. Cheng, D. Mewes, A. Luke, Boiling phenomena with surfactants and polymeric additives: a state-of-the-art review, Int. J. Heat Mass Transfer 50 (2007) 2744–2771.
[5] J.R. Thome, Boiling in microchannels: a review of experiment and theory, Int. J. Heat Fluid Flow 25 (2004) 128–139.
[6] L. Cheng, D. Mewes, Review of two-phase flow and flow boiling of mixtures in small and mini channels, Int. J. Multiphase Flow 32 (2006) 183–207.
[7] S.G. Kandlikar, Fundamental issues related to flow boiling in minichannels and microchannels, Exp. Therm. Fluid Sci. 26 (2002) 389–407.
[8] L. Cheng, G. Ribatski, J.R. Thome, Gas–liquid two-phase flow patterns and flow pattern maps: fundamentals and applications, ASME Appl. Mech. Rev. 61 (2008) 050802-1–050802-28.

[9] M.B. Ould-Didi, N. Kattan, J.R. Thome, Prediction of two-phase pressure gradients of refrigerants in horizontal tubes, Int. J. Refrigeration 25 (2002) 935–947.
[10] J. Moreno Quibén, J.R. Thome, Flow pattern based two-phase frictional pressure drop model for horizontal tubes, Part I: Diabatic and adiabatic experimental study, Int. J. Heat Fluid Flow 28 (2007) 1049–1059.
[11] J. Moreno Quibén, J.R. Thome, Flow pattern based two-phase frictional pressure drop model for horizontal tubes, Part II: New phenomenological model, Int. J. Heat Fluid Flow 28 (2007) 1060–1072.
[12] J. Moreno Quibén, Experimental and analytical study of two-phase pressure drops during evaporation in horizontal tubes, Ph.D. Thesis, Swiss Federal Institute of Technology (EPFL), Lausanne, Switzerland, 2005.
[13] L. Cheng, G. Ribatski, J. Moreno Quibén, J.R. Thome, New prediction methods for CO_2 evaporation inside tubes: Part I – A two-phase flow pattern map and a flow pattern based phenomenological model for two-phase flow frictional pressure drops, Int. J. Heat Mass transfer 51 (2008) 111–124.
[14] L. Cheng, G. Ribatski, J.R. Thome, New prediction methods for CO_2 evaporation inside tubes: Part II – An updated general flow boiling heat transfer model based on flow patterns, Int. J. Heat Mass transfer 51 (2008) 125–135.
[15] R.J. da Silva Lima, J. Moreno Quibén, C. Kuhn, T. Boyman, Ammonia two-phase flow in a horizontal smooth tube: flow pattern observations, diabatic and adiabatic frictional pressure drops and assessment of prediction methods, Int. J. Heat Mass Transfer 52 (2009) 2273–2288.
[16] REFPROP, NIST Refrigerant Properties Database 23, Gaithersburg, MD, 1998, Version 6.01.
[17] Z. Rouhani, E. Axelsson, Calculation of volume void fraction in a subcooled and quality region, Int. J. Heat Mass Transfer 17 (1970) 383–393.
[18] J.R. Taylor, An Introduction to Error Analysis, second ed., University Science Books, Mill Valley, 1997.
[19] F.W. Dittus, L.M.K. Boelter, Heat transfer in automobile radiators of tubular type, Univ. Calif. Publ. Eng. 2 (1930) 443–461.
[20] V. Gnielinski, New equations for heat and mass transfer in turbulent pipe and channel flow, Int. Chem. Eng. 16 (2) (1976) 359–368.
[21] L. Wojtan, T. Ursenbacher, J.R. Thome, Investigation of flow boiling in horizontal tubes: Part I – A new diabatic two-phase flow pattern map, Int. J. Heat Mass Transfer 48 (2005) 2955–2969.
[22] L. Wojtan, T. Ursenbacher, J.R. Thome, Investigation of flow boiling in horizontal tubes: Part II – Development of a new heat transfer model for stratified-wave, dryout and mist flow regimes, Int. J. Heat Mass Transfer 48 (2005) 2970–2985.
[23] N. Kattan, J.R. Thome, D. Favrat, Flow boiling in horizontal tubes. Part 1: Development of a diabatic two-phase flow pattern map, J. Heat Transfer 120 (1998) 140–147.
[24] L. Cheng, G. Ribatski, L. Wojtan, J.R. Thome, New flow boiling heat transfer model and flow pattern map for carbon dioxide evaporating inside tubes, Int. J. Heat Mass Transfer 49 (2006) 4082–4094.
[25] L. Cheng, G. Ribatski, L. Wojtan, J.R. Thome, Erratum to: new flow boiling heat transfer model and flow pattern map for carbon dioxide evaporating inside tubes, [Heat Mass Transfer 49 (21–22) (2006) 4082–4094], Int. J. Heat Mass Transfer 50 (2007) 391.